11th International Symposium on Turbulence and Shear Flow Phenomena (TSFP11)
Southampton, UK, July 30 to August 2, 2019

FLOW PHYSICS OF NORMAL AND ABNORMAL BIOPROSTHTETIC AORTIC VALVES

Jung Hee Seo

Department of Mechanical Engineering
Johns Hopkins University
Baltimore, Maryland, 21218, USA
jhseo@jhu.edu

Chi Zhu

Department of Mechanical Engineering
Johns Hopkins University
Baltimore, Maryland, 21218, USA
czhu19@jhu.edu

Jon Resar

Adult Cardiac Catheterization Laboratory
Johns Hopkins Hospital
Baltimore, Maryland, 21287, USA
jresar@jhmi.edu

Rajat Mittal

Department of Mechanical Engineering
Johns Hopkins University
Baltimore, Maryland, 21218, USA
mittal@jhu.edu

ABSTRACT

Flow physics of transvalvular flows in the aorta with bioprosthetic valves is investigated using computational modeling. For the efficient simulations of flow-structure-interaction in transvalvular flows, a simplified, reduced degree-of-freedom valve model is employed with a sharp-interface immersed boundary based incompressible flow solver. Simulations are performed for normal valves as well as valves with reduced leaflet motion that models the effect of early leaflet thrombosis. The structure of the aortic jet and the hemodynamic stresses on the aortic wall are analysed to understand the hemodynamic impacts and possible long-term clinical implications of sub-clinical reduced leaflet motion.

INTRODUCTION

Aortic valve replacement with a bioprosthetic valve has become highly prevalent. Recent clinical studies of bioprosthetic aortic valves based on high-resolution computed tomography (CT) scans, have however, shown a higher than expected incidence of reduced leaflet motion (RLM) due to early leaflet thrombosis (Makkar et al., 2015). In most cases, this early RLM in bioprosthetic valves is considered subclinical, i.e. it does not manifest any symptoms, and is difficult to detect. While it is apparent that severe RLM causing pressure drop of more than 20 mmHg is clinically significant (Pislaru et al., 2016), the hemodynamic impact and implication of sub-clinical RLM found in patients is still not clear. Interestingly, the sub-clinical RLM occurs asymmetrically (Makkar et al., 2015); only 1 or 2 leaflets are restricted, and this should introduce substantial changes in the transvalvular hemodynamics such as the jet direction and its impingement on the aortic wall. The hemodynamics associated with RLM, has however, not been comprehensively studied. In the present study, we investigate the transvalvular hemodynamics with various types of RLMs using computational modeling. The objective here is to derive hemodynamic metrics that can predict the clinical implications of RLMs, such as aorta remodeling.

For the computational investigation of transvalvular flow physics with normal and abnormal aortic valves, an efficient and easy-to-handle fluid-structure-interaction (FSI) model is needed. In the present study, we propose a simplified FSI model that requires fewer parameters and a lower computational cost for the efficient hemodynamic simulation of aortic valves. The proposed, reduced degree-of-freedom (DOF) model is focused on resolving the dominant kinematics of leaflet motions and the associated transvalvular hemodynamics rather than the detailed structural dynamics of the valve.

Using the reduced DOF valve model, the transvalvular hemodynamics for 1) baseline, normal, 2) RLM in 1 leaflet (RLM1), and 3) RLM in 2 leaflets (RLM2) cases are computationally investigated.

METHOD

In this study, a canonical model of aorta and prosthetic aortic valve are employed for the investigation of transvalvular flow physics. The aorta model is based on the data presented by Reul et al.(1990). Although there are many different types of bioprosthetic valves, here, we considered a simple and generic model as shown in Fig. 1. The FSI simulations for the transvalvular hemodynamics are performed with a sharp interface, immersed boundary method based incompressible flow solver.

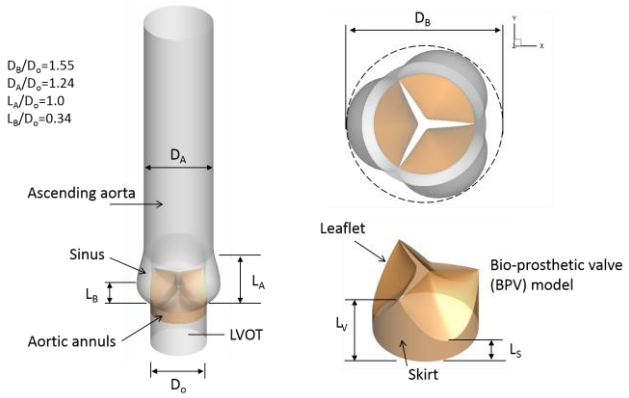

Figure 1. Geometrical models for the aorta and bio-prosthetic valve.

Reduced Degree of Freedom Valve Model

The simplified valve dynamics model proposed is a reduced degree-of-freedom (DOF) model. The key idea is decomposing the valve displacement (d_v) into a time coefficient and spatial modal vector;

$$\vec{d}_v(t,\vec{x}) = c(t)\vec{b}(\vec{x}), \qquad (1)$$

The spatial vector, b is prescribed by using the fully opened and fully closed valve geometries. Thus, the time coefficient, c represents the degree of opening. By integrating a simplified equation of motion over the leaflet surface, and applying the decomposition, Eq. (1), one can obtain the equation for the time coefficient, c:

$$\frac{d^2c}{dt^2} = \frac{\int \Delta p\, dS}{\int \alpha \vec{b}\cdot\vec{n}\, dS} - \frac{K}{\alpha}(c - c_0), \qquad (2)$$

where Δp is the net pressure force on the leaflet, α is a virtual mass coefficient, and K is a stiffness coefficient. The resulting model has two parameters (α,K) and 1 DOF (c) for each leaflet but can still resolve the leaflet motions by coupling with the full fluid dynamics equations. This model is computationally efficient because only 1 ordinary differential equation needs to be solved for each leaflet.

Flow Solver

The flow simulation for the FSI modeling is performed by a highly versatile, fully parallelized in-house immersed boundary, incompressible flow solver "ViCar3D" that computes flow with complex moving/deforming bodies (Mittal et al., 2008). The solver models flows via direct numerical simulation (DNS) as well as large-eddy simulation (LES) and employs an efficient, immersed boundary based Bi-conjugate gradient (BiCG) solver that scales well on up to about 1000 processors (Zhu et al., 2017). The solver has been extensively validated for a variety of laminar/turbulent flows and FSI problems and employed for a wide range of studies of cardiac hemodynamics, including modeling of hemodynamics in the left ventricle with natural and prosthetic mitral valves.

The flow through the aorta and valve model is driven by the prescribed, time-dependent blood flowrate at the inlet. In the present study, the flowrate profile is synthetized by the following function.

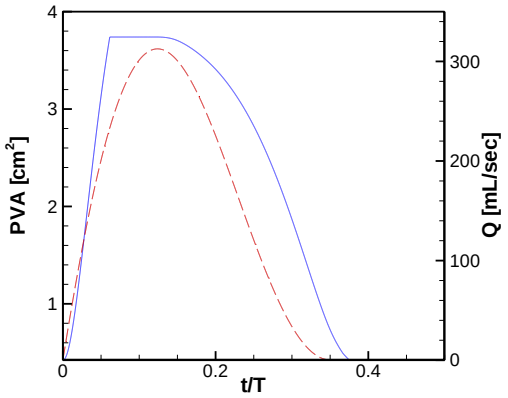

Figure 2. Time profiles of the projected valve opening area (PVA, solid line), and systolic flowrate (Q, dashed line).

$$Q(t) = (SV)\frac{\pi}{T_s^2}(T_s - t)\sin(\pi t / T_s), \qquad (3)$$

where SV is a stroke volume, and T_s is a systolic time duration. The net pressure force on the leaflet obtained from the flow solution is used to solve Eq. (2) for the valve dynamics, and the valve displacement and velocity provide boundary conditions for the flow solver.

RESULTS

Aortic flow simulations with the bioprosthetic valve models are performed for baseline normal, RLM1, and RLM2 cases. For the baseline case with normal leaflet motion, the following parameters are used: the valve size, which is the same as the aortic root diameter is chosen to be D_0=23 mm and the stroke volume is set to SV=60 mL based on the post aortic valve replacement patient data (Barletta et al., 2018). The heart rate and systolic time duration (T_s) are set to 60 BPM and 0.35 sec, respectively. The peak flow Reynolds number based on the aortic root diameter (D_0) is about 4300. The baseline parameters for the reduced DOF valve model determined by comparing the time profile of valve opening area with the experimental data (Tullio and Pascazio, 2016) are α=40 kg/m^3 and K=10 kPa/m.

For the RLM1 (RLM in 1 leaflet) case, to model the leaflet affected by the early thrombosis, the stiffness parameter, K is increased by 10 times to 100 kPa/m on one leaflet. Likewise, for the RLM2 (RLM in 2 leaflets) case, K is increased by 10

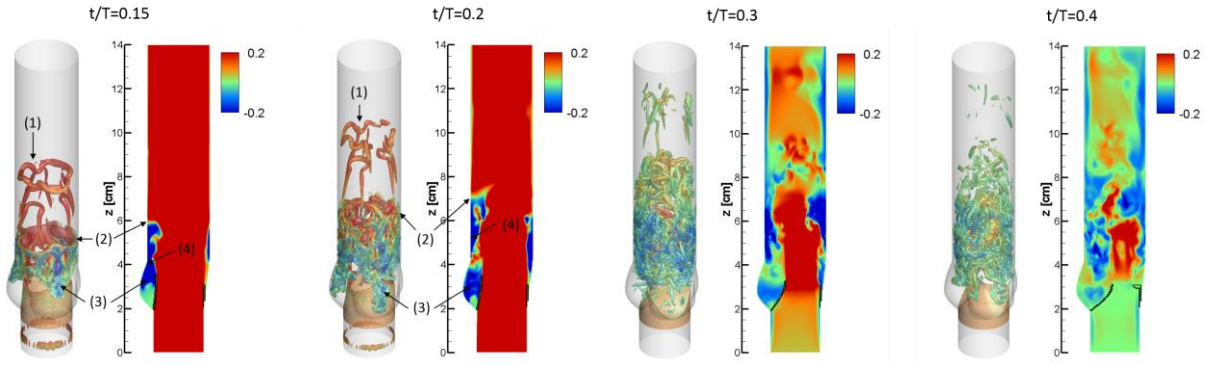

Figure 3. Three-dimensional vortical structures visualized by Q-criteria and the axial velocity contours for the baseline (normal) case. Flow features noted: (1) primary vortex ring, (2) flow attachment, (3) reverse flow, and (4) circulation bubble.

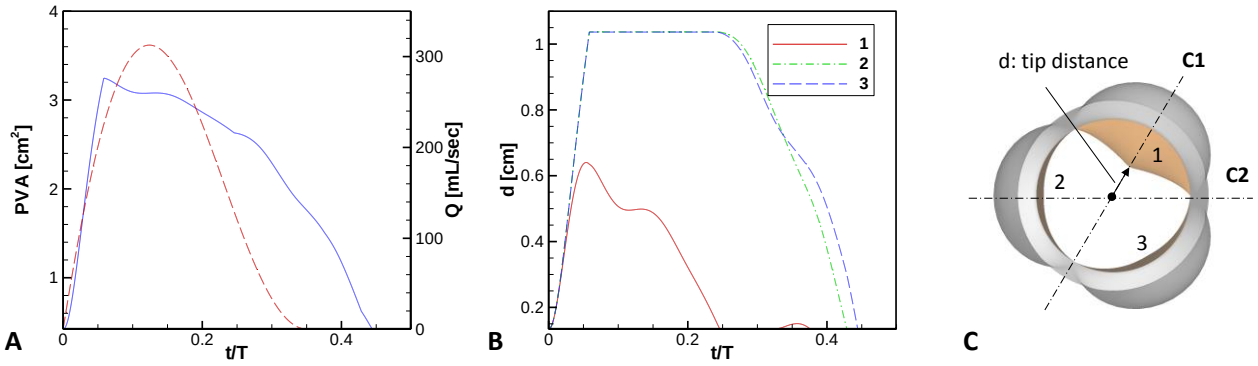

Figure 4. A: Time profiles of the projected valve opening area (PVA, solid line), and systolic flowrate (Q, dashed line) for the RLM1 case. B: Time profiles of the distance from the valve centre to the tip of each leaflet (d). C: Schematic showing the leaflet number, the tip distance, and the location of cross-sectional planes.

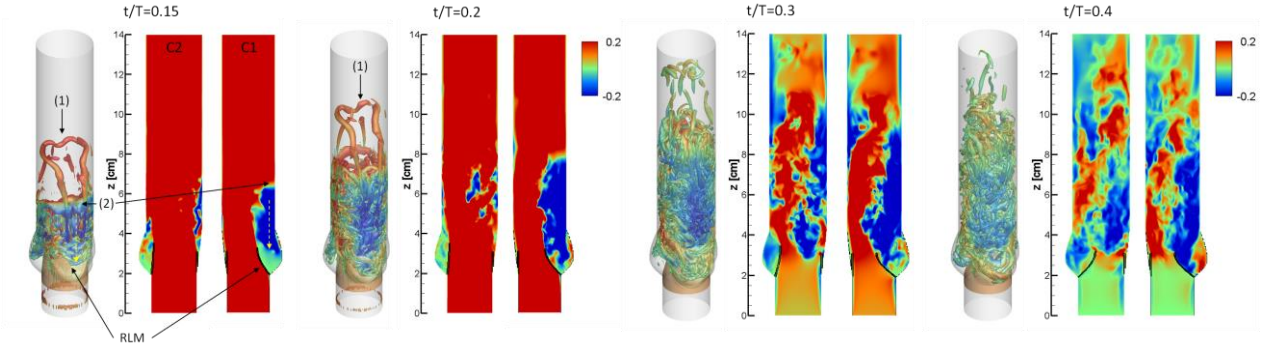

Figure 5. Three-dimensional vortical structures visualized by Q-criteria and the axial velocity contours on two cross-sectional planes (C1 and C2, see Fig. 4C) for RLM1 case. Reduced motion leaflet is marked by 'RLM'. Flow features noted: (1) primary vortex ring, (2) flow attachment.

times on two leaflets.

Normal

The simulation results for the baseline, normal case are presented in Figs. 2 and 3. Figure 2 shows the time profiles of the systolic flowrate and projected valve opening area (PVA). With the acceleration of systolic flow, the valve opens rapidly and is fully open at around t/T=0.06. It remains fully open and starts to close at t/T=0.125, when the flow starts to decelerate. The valve subsequently starts to close and is fully closed at around t/T=0.375.

The transvalvular flow fields are visualized in Fig. 3 for the three-dimensional vortex structures and axial velocity contours at several time instances. Initially the transvalvular flow is like a jet, but during the deceleration phase, additional flow features including the attachment and circulation bubble are observed. The axial velocity contours in Fig. 3 are plotted with truncated contour range to show those flow patterns more clearly. At t/T=0.15, the primary vortex ring (marked by (1)) generated during the acceleration phase is clearly visible, but one can see the additional flow features marked by (2), that are due to the attachment of the transvalvular jet on the aortic wall. This generates a flow structure like a re-circulation bubble (4), and inside the bubble, a reverse flow is observed (3). The circulation bubble makes the flow into the aortic sinuses. At t/T=0.2, the attachment point propagates downstream as the circulation bubble grows. As one can see in the 3D vortical structure, the reverse flow forms a jet near the center of each sinus, and it flows into the sinus. As flow decelerates further, the reverse pressure gradient makes the flow unstable, and the shear layer of circulation bubble roles into vortices and eventually breaks into smaller vortical structures as shown at t/T=0.3. After the valve is fully closed, the vortical structures in the aorta are slowly decaying (t/T=0.4).

The jet attachment, formation of circulation bubble, and the reverse flow into the sinus may play important roles on the sinus washout and the blood supply into the coronary arteries.

RLM in 1 leaflet (RLM1)

Figure 4A shows the time profiles of the systolic flowrate and projected valve opening area (PVA) for the RLM1 case. The motion of each leaflet is presented by the tip distance (distance from the valve centre to the tip of each leaflet, see Fig. 4C) in Fig. 4B. Due to the increased stuffiness, the motion of one leaflet (leaflet 1, see Fig. 4C) is noticeably reduced. It opens only up to about 60% of the normal leaflets and closes early at around t/T=0.25. Because of this reduced motion of 1 leaflet, the maximum PVA is slightly decreased to 3.25 cm^2 from 3.74 cm^2 of the baseline normal case.

The transvalvular flow fields for the RLM1 case are visualized in Fig. 5 for the three-dimensional vortex structures and axial velocity contours on two cross sectional planes, C1 (across the reduced motion leaflet) and C2 (across one of the normal leaflets) shown in Fig. 4C. One can see several flow

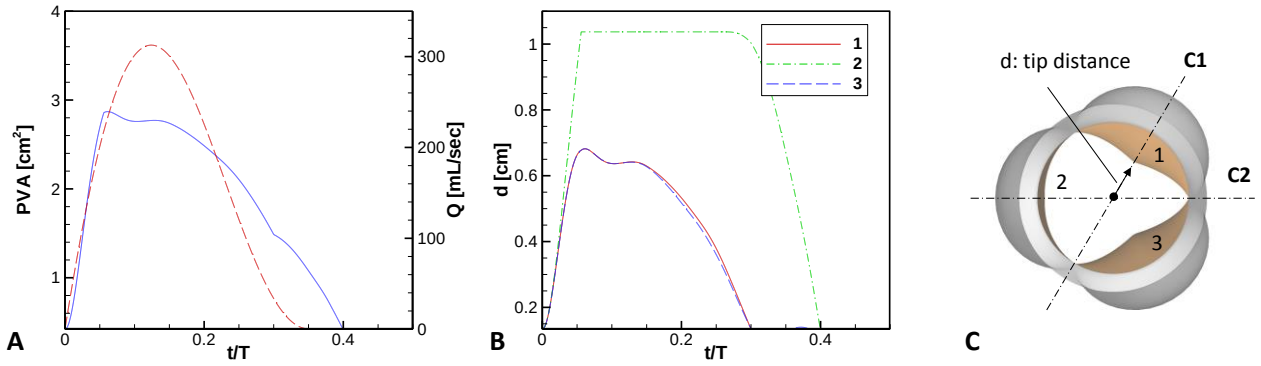

Figure 6. A: Time profiles of the projected valve opening area (PVA, solid line), and systolic flowrate (Q, dashed line) for the RLM2 case. B: Time profiles of the distance from the valve centre to the tip of each leaflet (d). C: Schematic showing the leaflet number, the tip distance, and the location of cross-sectional planes.

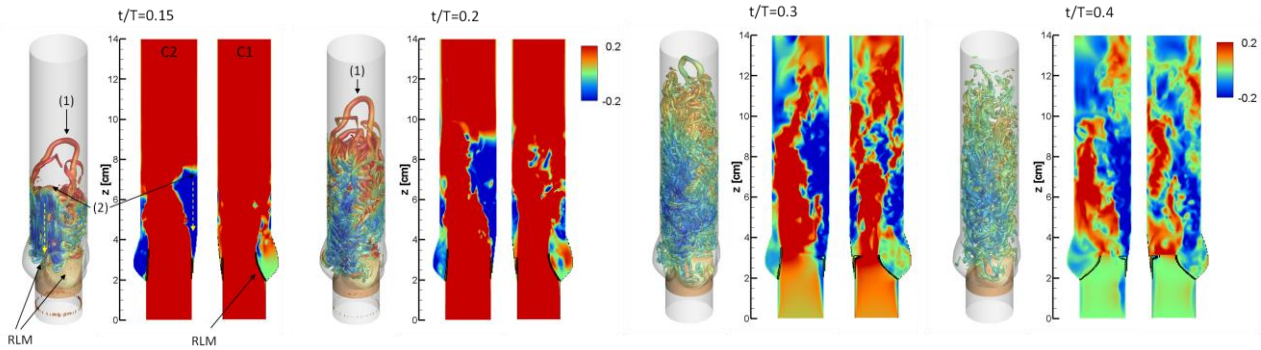

Figure 7. Three-dimensional vortical structures visualized by Q-criteria and the axial velocity contours on two cross-sectional planes (C1 and C2, see Fig. 6C) for RLM2 case. Reduced motion leaflets are marked by 'RLM'. Flow features noted: (1) primary vortex ring, (2) flow attachment.

features altered by the RLM. The primary vortex ring at t/T=0.15 (marked by (1)) generated during the acceleration phase is tilted and the ring is stretched to the reduced motion leaflet side. As shown in Fig. 5, the direction of aortic jet is also titled toward the wall opposite to the reduced motion leaflet, and this generates large separation bubble at the downstream to the reduced motion leaflet (C1, t/T=0.15). The vortical structure associated with the re-attachment flow (marked by (2)) becomes stronger. As the attachment point propagates downstream (t/T=0.2), the circulation bubble grows rapidly, and its size is much bigger than the one for the normal case. On the other hand, the circulation bubble on the normal leaflet side in RLM1 becomes smaller. As a result, the reverse flow into the sinus is much stronger on the reduced motion leaflet side than the normal leaflet sides. At t/T=0.3, because of the tilting of aortic jet and the big separation bubble on the reduced motion leaflet side, the overall flow pattern forms a large-scale clockwise circulation as shown in the cross-sectional plane, C1 at t/T=0.3. All leaflets are closing at t/T=0.4, and the vortical structures are decaying, but the overall circulation flow pattern still remains in the aorta.

RLM in 2 leaflets (RLM2)

The time profiles of the projected valve opening area (PVA) and the tip distances to each leaflet for the RLM2 case are plotted in Fig. 6A&B. As one can see in Fig. 6B, two leaflets (1 and 3) are stiffened and their motion is reduced. The maximum tip distances for those two leaflets are about 60% of the normal leaflet. The reduced motion leaflets start to close right after the peak of systolic flow (t/T=0.15), and closes early at around t/T=0.3, while the normal leaflet starts to close in the deceleration phase after two reduced motion leaflets are closed, and the normal leaflet is fully closed at t/T=0.4. Due to the RLM on two leaflets, the maximum PVA for RLM2 is further decreased to 2.87 cm^2, and this increases the aortic jet velocity.

The flow structures for the RLM2 case are presented in Fig. 7. Similarly to the RLM1 case, the primary vortex ring (marked by (1)) is titled, but it is stretched to the mid-location of two reduced motion leaflets. The direction of aortic jet is shifted toward the one normal leaflet side (t/T=0.15, C2), and this generates a separation bubble on the downstream wall between two reduced motion leaflets. The strong attachment flow (marked by (2)) and reverse flow are thus also observed in the middle of two reduced motion leaflets. Because of this aortic jet shifting, the circulation bubble and the reverse flow into the sinus associated with the reduced motion leaflets are smaller and weaker (t/T=0.15, C1) than the RLM1 case.

At t/T=0.2, the circulation bubble formed on the downstream wall between two reduced motion leaflets grows but its shape is quite different from the one formed directly downstream to the reduced motion leaflet in the RLM1 case. The tilting of the aortic jet and the separation bubble again form a large scale, clockwise circulation flow pattern at t/T=0.3. Note that, due to the further reduced valve opening area, the aortic jet becomes stronger and it results in more energetic

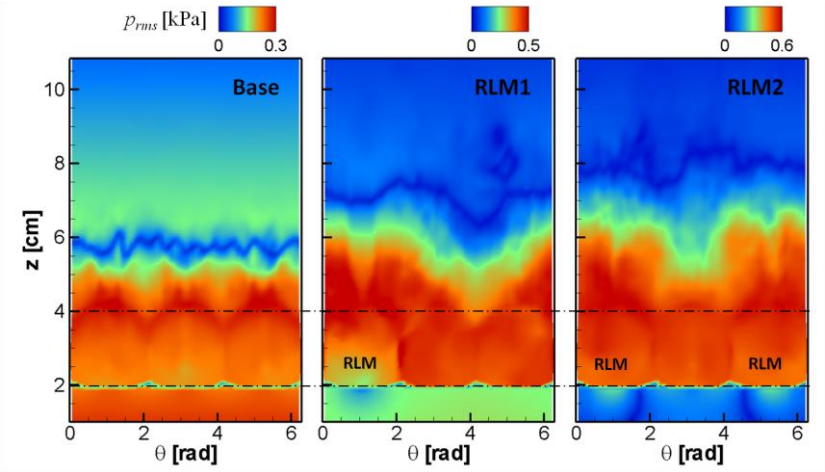

Figure 8. Distributions of root-mean-squared (rms) wall pressure fluctuation (p_{rms}) on the aortic wall for normal (Base), RLM1, and RLM2 cases. Sinus region is denoted with dash-dot lines. Sinus associated to the reduced motion leaflet is marked with 'RLM'.

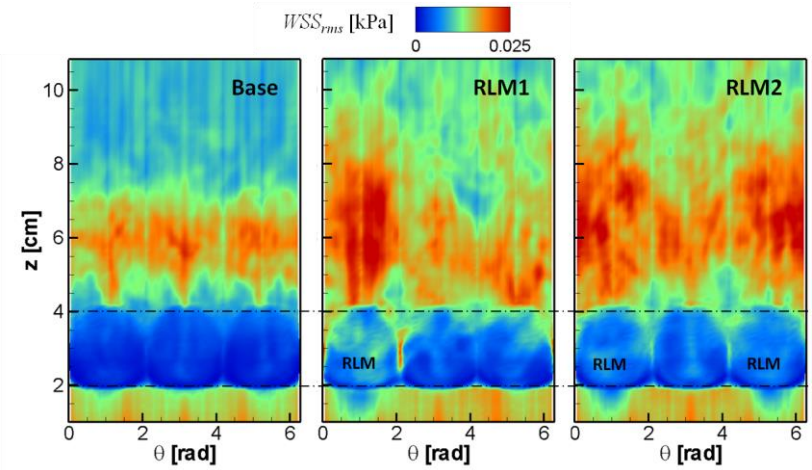

Figure 9. Distributions of root-mean-squared (rms) wall shear stress fluctuation (WSS_{rms}) on the aortic wall for normal (Base), RLM1, and RLM2 cases. Sinus region is noted with dash-dot lines. Sinus associated to the reduced motion leaflet is marked with 'RLM'.

vortical structures, that breaks into smaller structures as shown at t/T=0.3 & 0.4. Even after all leaflets are closed at t/T=0.4, the aortic flow still remains energetic.

Hemodynamic stresses

The RLM cases considered in this study are sub-clinical as the valve opening area decreased by only 13% for RLM1, and 23% for RLM2. The pressure drop across the valve at the peak systole is about 1.2 mmHg for the normal case, and this increased to 3 mmHg for RLM1 and 4 mmHg for RLM2, but these values are considered sub-clinical.

As shown above, however, the RLM not only decreases the valve opening area and thus increases the aortic jet strength, but also substantially changes the aortic flow patterns. For 1 or 2 leaflets RLM cases, the asymmetry between the leaflet motions tilts the direction of the aortic jet, which generates the bigger separation bubble and the stronger attachment flow on the aortic wall downstream to the reduced motion leaflets. These modified flow patterns should have considerable effects especially on the hemodynamic stresses on the aortic wall. To investigate this, the wall normal, pressure stresses and the tangential, viscous shear stresses are calculated by using the simulation results. Particularly, we are interested in the temporal fluctuation of those stresses due to the unsteady, turbulent flows in the aorta. The root-mean-squared (rms), wall pressure fluctuation is calculated by

$$p_{rms} = \sqrt{\frac{1}{T}\int (p-\bar{p})^2 dt}\,, \tag{4}$$

where T is the period of a cardiac cycle and bar denotes time average over the cardiac cycle. The wall shear stress (WSS) and its rms are calculated by

$$WSS = \left|\mu \frac{\partial \vec{u}}{\partial n}\right|,\ WSS_{rms} = \sqrt{\frac{1}{T}\int \left(WSS - \overline{WSS}\right)^2 dt}\,, \tag{5}$$

where n denotes wall normal direction.

The spatial distributions of p_{rms} and WSS_{rms} are shown in Figs. 8&9 for the normal, RLM1, and RLM2 cases. In general, the wall pressure fluctuations are strong on the sinus wall and the near downstream aortic wall. With RLM, the wall pressure fluctuation increases on the downstream of the reduced motion leaflet. The peak value of p_{rms} is about 0.3 kPa, and this increased to 0.5 kPa for RLM1, and 0.6 kPa for RLM2. Interestingly, the region of strong wall pressure fluctuation falls

into the region inside the separation bubble. The WSS fluctuation is weak on the sinus wall but strong on the downstream aortic wall (about 2 cm downstream to the sinus). As one can expect, the peak WSS fluctuation is observed around the flow re-attachment region. Similarly to the wall pressure fluctuation, the RLM increases the WSS fluctuation especially on the downstream to the reduced motion leaflets. Although the peak values of WSS_{rms} are similar for all 3 cases (about 0.035 kPa), the region of high WSS_{rms} is clearly increased with RLM as shown in Fig. 9. Overall, the RLM increases both wall pressure and WSS fluctuations on the aortic wall downstream to the reduced motion leaflet, and the asymmetric leaflet motion also causes the asymmetry on the hemodynamic stresses on the aortic wall.

CONCLUSION

In this study, transvalvular hemodynamics with normal and abnormal prosthetic aortic valves are computationally investigated. The subclinical, reduced leaflet motion due to early leaflet thrombosis is considered on 1 and 2 leaflets. The simulation results have shown that the reduced leaflet motion tilts the direction of aortic jet and generates stronger flow separation and re-attachment flow on the aortic wall downstream to the reduced motion leaflets. These changes on the flow pattern increase both wall pressure and shear stress fluctuations on the downstream aortic wall. Additionally, the asymmetry on the leaflet motion results in asymmetric, hemodynamic stress distribution on the aorta wall. Although the subclinical RLMs may clinically insignificant in terms of transvalvular hemodynamic load, the modified hemodynamic stresses on the aortic wall may have long-term clinical implications, especially for the aorta wall damage and remodelling.

REFERENCES

Barletta, G., Venditti, F., Stefano, P., Del Bene, R. and Di Mario, C., 2018. "Left ventricular outflow tract shape after aortic valve replacement with St. Jude Trifecta prosthesis," *Echocardiography*, Vol. 35(3), pp.329-336.

Makkar, R.R., Fontana, G., Jilaihawi, H., Chakravarty, T., Kofoed, K.F., De Backer, O., Asch, F.M., Ruiz, C.E., Olsen, N.T., Trento, A. and Friedman, J., 2015. "Possible subclinical leaflet thrombosis in bioprosthetic aortic valves," *New England Journal of Medicine*, Vol. 373(21), pp.2015-2024.

Mittal, R., Dong, H., Bozkurttas, M., Najjar, F.M., Vargas, A. and von Loebbecke, A., 2008. "A versatile sharp interface immersed boundary method for incompressible flows with complex boundaries," *Journal of computational physics*, Vol. 227(10), pp.4825-4852.

Pislaru, S.V., Nkomo, V.T. and Sandhu, G.S., 2016. "Assessment of prosthetic valve function after TAVR," *JACC: Cardiovascular Imaging*, Vol. 9(2), pp.193-206.

Reul, H., Vahlbruch, A., Giersiepen, M., Schmitz-Rode, T.H., Hirtz, V. and Effert, S., 1990. "The geometry of the aortic root in health, at valve disease and after valve replacement," *Journal of biomechanics*, Vol. 23(2), pp.181-191.

de Tullio, M.D. and Pascazio, G., 2016. "A moving-least-squares immersed boundary method for simulating the fluid-structure interaction of elastic bodies with arbitrary thickness," *Journal of Computational Physics*, Vol. 325, pp.201-225.

Zhu, C., Seo, J.H., Vedula, V. and Mittal, R., 2017. "A Highly Scalable Sharp-Interface Immersed Boundary Method for Large-Scale Parallel Computers," *In 23rd AIAA Computational Fluid Dynamics Conference* (AIAA 2017-3622).